Cellulose (2017) 24:5371–5387
DOI 10.1007/s10570-017-1524-2

ORIGINAL PAPER

Esterification of bagasse cellulose with metal salts as efficient catalyst in mechanical activation-assisted solid phase reaction system

Tao Gan · Yanjuan Zhang · Yang Su · Huayu Hu · Aimin Huang · Zuqiang Huang · Dong Chen · Mei Yang · Juan Wu

Received: 17 July 2017 / Accepted: 10 October 2017 / Published online: 16 October 2017

Abstract The present study focused on investigating the catalytic mechanism of metal salts (sodium hypophosphite, sodium bisulfate and ammonium ferric sulfate) for esterification of bagasse cellulose carried out by mechanical activation-assisted solid phase reaction in a stirring ball mill. FTIR analysis of the products confirmed that these metal salts could catalyze the esterification of cellulose. XRD, SEM, FTIR, and ^{31}P-NMR analyses of different samples indicated a synergistic effect between metal salt and ball milling, and the presence of metal salts enhanced the destruction on crystal structure of cellulose by mechanical force. The catalytic mechanism of three metal salts was difference: sodium bisulfate and ammonium ferric sulfate belonged to the catalytic mechanism of protonic acid and Lewis acid, respectively, while the catalytic mechanism of sodium hypophosphite was considered as that it could react with maleic acid to form active intermediates under ball milling.

Keywords Cellulose · Esterification · Metal salt · Catalytic mechanism · Mechanical activation

Introduction

Sugarcane bagasse is an abundant and renewable source of lignocellulosic biomass and cellulose is one of the main components. Bagasse cellulose can be used for the preparation of environmentally friendly and biocompatible products. Because of the characteristics of biodegradability and sustainability, cellulose based materials have been widely used in daily life (Abhilash and Singh 2008; Chundawat et al. 2011). The molecules of cellulose are linear polymer of β-1,4-glycosidic bonds linked D-glucopyranose residues, and each base ring contains three hydroxyl groups in the repeating units (Lam and Luong 2014), which can be dramatically modified by the substitution reactions. Esterification is usually used for chemical modification of cellulose with acid anhydride or fatty acid to improve its properties. However, native cellulose with strong inter- and intramolecular hydrogen bonding has highly-ordered crystal structure and compact network structure, which make it resists

Electronic supplementary material The online version of this article (doi:10.1007/s10570-017-1524-2) contains supplementary material, which is available to authorized users.

T. Gan · Y. Zhang (✉) · Y. Su · H. Hu · A. Huang · Z. Huang (✉) · M. Yang · J. Wu
School of Chemistry and Chemical Engineering, Guangxi University, Nanning 530004, China
e-mail: zhangyj@gxu.edu.cn

Z. Huang
e-mail: huangzq@gxu.edu.cn

D. Chen
State Key Laboratory of Non-Food Biomass and Enzyme Technology, Guangxi Academy of Sciences, Nanning 530007, China

assault of other reagents (Nishiyama et al. 2002). Conventional synthetic methods include pyridine-acyl chloride method (Cr Py et al. 2009; Granstrom et al. 2011; Uschanov et al. 2011) and ester exchange method (Cao et al. 2013; Dankovich and Hsieh 2007). Pyridine-acyl chlorides are toxic and corrosive, and can be very easily inactived because of the water absorptivity, while ester exchange method consumes a large number of reagents. Therefore, these two methods are difficult to achieve industrial production, and many researchers began to explore the synthesis method of using fatty acids as esterifying agents instead of acyl chlorides. However, the reactivity of fatty acids and the nucleophilicity of hydroxyls in cellulose are poor, so the esterification of cellulose with fatty acids is difficult to take place. Two main methods can enhance the reactivity of fatty acids. One is using co-reactants (e.g., trifluoroacetic anhydride, p-toluenesulfonyl chloride, acetic anhydride, etc.) to react with fatty acids to form highly active mixed acid anhydrides, which then react with the hydroxyl groups of cellulose to produce cellulose esters (Granstrom et al. 2008; Hu et al. 2015; Huang et al. 2011). The other is using catalysts to accelerate the esterification, such as the addition of sodium hypophosphite could effectively enhance the esterification of cellulose with polycarboxylic acid (Gillingham et al. 1999; Morris et al. 1996). These esterification reactions are generally carried out in water, organic solvents, or ionic liquid, which present the disadvantages of complex procedure and difficulty in the purification of products and recovery of solvents.

With the increasing concerns on environmental protection, solid phase reaction (SPR) has attracted much attention. SPR is an efficient and green method due to the advantages of nonuse of solvent, high selectivity and yield, simple process, low energy consumption, and environmental friendliness (Crawford et al. 2015; James et al. 2012). However, SPR is different from liquid phase reaction as the mixing and contact of solid materials are not sufficient, limiting the energy exchange and diffusion of solid materials. So the reaction can only carry out at the interface between solid reactants. To overcome the problem of poor mass and heat transfer between solid materials and low chemical reactivity of highly crystalline cellulose, mechanical activation (MA) can be used as an assisted means for SPR. MA can break the compact network structure and stable crystal structure of cellulose and a part of mechanical energy may be transformed into internal energy of cellulose, which thus improve its reactivity. Moreover, MA can accelerate the diffusion and improve the contact status between reactants, contributing to enhancing the reaction efficiency (Huang et al. 2012a).

At present, using metal salts as catalyst for esterification are commonly applied in liquid phase reactions, and the catalytic mechanism mainly plays the catalytic role of Lewis acid or protonic acid (Barbosa et al. 2006; Bassan et al. 2013). For example, tri-butyl citrate was synthesized from citric acid and butanol catalyzed by heteropolyacid organic salts, and the catalytic mechanism is proton acid (Leng et al. 2009). Metal salts are mainly used as the non-derivative solvents and hydrolysis catalyst for cellulose (Kim et al. 2016; Morales-delaRosa et al. 2014), but they are seldom used in the chemical modification of cellulose. In our previous works, we found that adding appropriate amount of metal salts effectively improved the esterification of cellulose and lignocellulose by MA-assisted SPR (MASPR) (Huang et al. 2012b; Zhang et al. 2014). Although in the conditions of solid phase and lower temperature, the addition of metal salts was so efficient for esterification, considered that metal salts exhibit catalytic action induced by ball milling in SPR and the effects of MA and metal salts on the modification of these natural polymers are synergistic interaction.

The present study focused on investigating the catalytic mechanism of metal salts for the esterification of bagasse cellulose by MASPR in a stirring ball mill. Three kinds of metal salts, sodium bisulfate ($NaHSO_4$), ammonium ferric sulfate ($NH_4Fe(SO_4)_2$), and sodium hypophosphite (NaH_2PO_2), were applied as catalyst for the maleation of cellulose with maleic acid as esterifying agent. In addition, the effects of different metal salts on the molecular structure of cellulose and maleic acid treated by MA and MA + metal salt (MAMS) in the same equipment and conditions of MASPR were comparatively investigated. X-ray diffraction (XRD), scanning electron microscopy (SEM), Fourier transform infrared spectroscopy (FTIR), and ^{31}P-nuclear magnetic resonance (^{31}P-NMR) analyses were applied to characterize the resulting samples to explore the catalytic mechanism of metal salts in MASPR system.

Experimental

Materials

Cellulose material used in this study was separated from sugarcane bagasse (cellulose content of 41.30 wt%), supplied by a local sugar factory (Nanning, China). The separation and purification of cellulose were according to the reported method (Rowell 1994), and the cellulose content of the resulting bagasse cellulose was over 98.49 wt% with a degree of polymerization of 563. Maleic acid, sodium hypophosphite, sodium bisulfate, ammonium ferric sulfate, anhydrous ethanol, and other reagents were of analytical grade without further purification and obtained from commercial sources.

Preparation of esterified cellulose by MASPR

Preparation of esterified cellulose by MASPR was performed in a customized stirring ball mill, and the schematic diagram is shown in Fig. 1. Fixed amount of milling balls (500 mL, 5 mm diameter) was first added into a jacketed stainless steel chamber (1200 mL), and then 10.0 g of cellulose, 75 wt% (weight percent compared to cellulose) of maleic acid (esterifying agent), and 10 wt% (weight percent compared to cellulose) of metal salt (catalyst) were added into the chamber. The mixture was subjected to milling at the speed of 300 rpm under a constant temperature of 80 °C by circulating the thermostatic water in the jacket of chamber. When milled for different designated time, the balls were removed from the milled material. The material was first washed to neutral with distilled water to remove metal salt and unreacted reagents, and then with absolute alcohol to prevent cellulose hornification in the presence of water when vacuum-dried at 55 °C. After dried for 48 h, the resulting products were obtained and sealed for analysis.

MA and MAMS treatments of cellulose and maleic acid

MA and MAMS treatments of cellulose and maleic acid were carried out in the same equipment as in MASPR, and the milling conditions were also the same as in MASPR except for the addition of reagents. For MA treatment of cellulose and maleic acid, 10.0 g of cellulose or maleic acid was added in the chamber for milling without any other reagent. For MAMS treatment of cellulose or maleic acid, 10.0 g of cellulose or maleic acid with 10 wt% of metal salt (weight percent compared to cellulose or maleic acid) were added into the chamber. MA treated cellulose and maleic acid and MAMS treated maleic acid were directly sealed for characterization. MAMS treated cellulose was first washed with distilled water to remove metal salt, and then with absolute alcohol to prevent cellulose hornification. After vacuum-dried at 55 °C for 48 h, the resulting samples were obtained and sealed for characterization.

Determination of carboxyl content

The degree of esterification of maleated cellulose was determined by measuring the quantity of introduced carboxyl groups. The content of carboxyl groups (C_{COOH}) in modified cellulose was measured by titration method as follows (Jr. Karnitz et al. 2007):

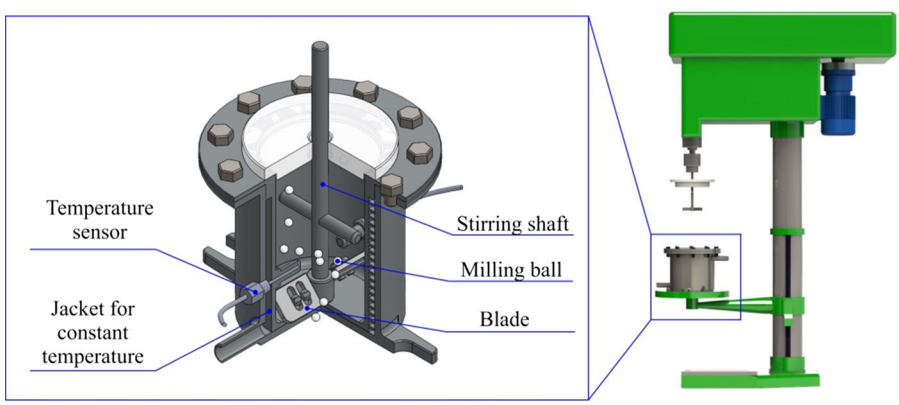

Fig. 1 Schematic diagram of stirring ball mill

0.1 g (precision 0.1 mg) of modified cellulose was treated with 100.0 mL of aqueous NaOH solution (0.01 mol L^{-1}) in a 250 mL Erlenmeyer for 1.0 h under constant stirring. The mixture was separated by filtration, and then three aliquots (25.0 mL) of the filtrate were titrated with standard aqueous HCl solution (0.01 mol L^{-1}). C_{COOH} was calculated by the following equation:

$$C_{COOH} = \frac{(V_{NaOH} \times C_{NaOH}) - 4 \times (V_{HCl} \times C_{HCl})}{m}$$

where C_{NaOH} (mmol L^{-1}) is the concentration of NaOH solution, C_{HCl} (mmol L^{-1}) is the concentration of HCl solution, V_{NaOH} (L) is the volume of NaOH solution, V_{HCl} (L) is the volume of HCl solution used for titration, and m (g) is the weight of maleated cellulose.

Hydroxamic acid test for qualitative measurement of acid anhydride

The sample was added to 0.5 mL of 1 M hydroxylamine hydrochloride methanol solution. The mixture was heated to boiling, and then a drop $FeCl_3$ solution (10 wt%) was added after cooling to 30 °C. The appearance of the characteristic color (bluish red color) of hydroxamic acid iron complex compound indicated the presence of acid anhydride.

Chemical characterization

The effects of different metal salts on the molecular structure of cellulose and maleic acid treated by MA and MA + metal salt (MAMS) in MASPR system were comparatively investigated. The products were characterized by XRD, SEM, FTIR, and ^{31}P-NMR. The operating conditions of these analyses were described in Supplementary Material.

Results and discussion

Esterification of cellulose catalyzed by metal salts in MASPR system

The reaction efficiency was determined by measuring the amounts of substituent groups in the products. The carboxyl contents of different modified cellulose samples are presented in Table 1. With the assistance of metal salts and MA, maleated cellulose was successfully prepared by SPR. The catalytic effect of NaH_2PO_2 was better than other two metal salts. The carboxyl content of modified cellulose increased as the increase of milling time, and reached a value of 3.577 mmol g^{-1} at 120 min. It was clearly observed that metal salts had a good catalytic effect on maleation of cellulose in MASPR system. Compared with conventional synthetic methods, MASPR is a fast and facile method by carrying out the activation treatment and reaction simultaneously. Moreover, there is the absence of harmful solvents, and it is no loss of raw materials and pollution-free because the unreacted reagents can be recycled by ethanol and water washing.

Qualitative and quantitative analysis of cellulose by FTIR technology has been widely used, as the absorption band position and peak intensity of the infrared spectrum can quickly and accurately determine the effect of various treatments on the chemical structure of cellulose (Fumagalli et al. 2013). FTIR spectra of the cellulose before and after esterification by MASPR are presented in Fig. 2. Characteristic absorption peaks for vibration of lignin aromatic ring at 1513 and 1603 cm^{-1} are absence in Fig. 2a, indicating that the material did not contain lignin (Sun et al. 2000). The peaks at 1630 cm^{-1} are attributed to H–O–H bending of the adsorbed water. The untreated bagasse cellulose presents the infrared bands of usual cellulose already described in literature (Morán et al. 2008). The main characteristic absorption bands of plant cellulose are presented in Fig. 2a, including O–H (3000–3600 and 1300–1450 cm^{-1}), C–H (2900 cm^{-1}), and C–O (950–1200 cm^{-1}), which confirm the successful separation of cellulose from bagasse. Compared with the spectrum of Fig. 2a, several new peaks appear in the spectra of Fig. 2b–e. The peaks at 1731 and 1580 cm^{-1} are attributed to C=O stretching vibration of the ester linkage and the carboxylate groups (conjugated form), respectively (Sehaqui et al. 2017). The stretching vibration peaks of C=C (maleate), C–O–C (ester), and γ(CH) bending present at 1640, 1213, and 823 cm^{-1}, respectively. Moreover, the intensity of the absorption peak at 1731 cm^{-1} gradually increased for the modified cellulose catalyzed by $NaHSO_4$, $NH_4Fe(SO_4)_2$, and NaH_2PO_2, which was stronger than the that of the modified cellulose without any catalyst. These phenomena prove that maleated cellulose had been

Table 1 Carboxyl content of different modified cellulose samples

Metal salt	Milling time (min)	Carboxyl content (mmol g^{-1})
No catalyst	60	0.4883
	120	0.7415
NaHSO	60	1.639
	120	2.571
$NH_4Fe(SO_4)_2$	60	1.912
	120	3.095
NaH_2PO_2	60	2.383
	120	3.577

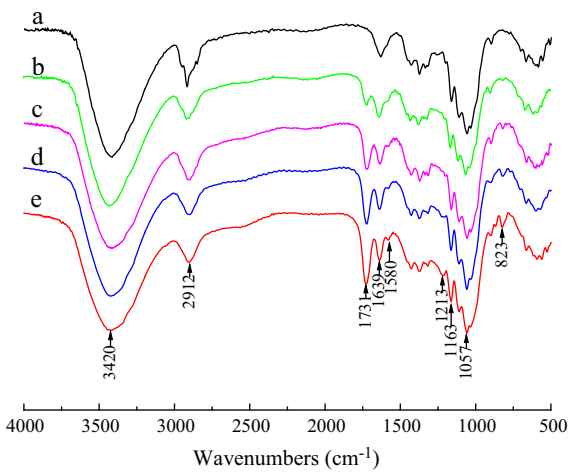

Fig. 2 FTIR spectra of **a** control cellulose and maleated cellulose, **b** without catalyst and catalyzed by **c** $NaHSO_4$, **d** $NH_4Fe(SO_4)_2$, and **e** NaH_2PO_2 with milling time = 120 min

successfully produced by MASPR, and NaH_2PO_2 exhibited the best catalytic effect. In order to further explore the catalytic mechanism of these three kinds of metal salts for the esterification of cellulose in MASPR system, effects of metal salts on the structure of cellulose and maleic acid were investigated by comparative analysis of the structural changes of MA and MAMS treated cellulose and maleic acid in the same equipment and conditions of MASPR.

Effect of metal salts on the structure of cellulose

FTIR analysis

The chemical structure of MA and MAMS treated cellulose with different milling time was investigated by FTIR, and the spectra are presented in Fig. 3. Compared with the spectrum of original cellulose, no new absorption peaks appear in the spectra of MA and MAMS treated cellulose samples, indicating that no new functional groups were generated or grafted by MA or MAMS treatment. However, the peak at 4000–2890 cm^{-1}, related with hydrogen-bonded O–H stretching vibration, shifted to a higher wavenumber as the increase of milling time, indicating that the stable structure of cellulose was destroyed by ball milling and the hydrogen bond energy of treated cellulose was higher than that of untreated one. Moreover, after MA + $NaHSO_4$, MA + $NH_4Fe(SO_4)_2$, and MA + NaH_2PO_2 treatments, the peak of O–H stretching vibration shifted to a higher wavenumber than that of only MA treatment. This demonstrates that metal salts could increase the internal energy of cellulose, resulting from the breakage of inter- and intramolecular hydrogen bonds and increase of free hydroxy groups in main chains of cellulose under intensive impact of mechanical actions, and then intermolecular hydrogen bonds were reformed by part of these free hydroxy groups.

The changes in hydrogen bond energy (ΔE) and the infrared Total Crystallinity Index (TCI) of control cellulose and different treated cellulose samples were determined based on the corresponding FTIR spectra, and the values are presented in Table 2. TCI of MA treated cellulose decreased with the increase of milling time, while ΔE increased with milling time, which confirm that MA treatment could increase the internal energy of cellulose and weaken the stability of hydrogen bond, leading to promote the reaction between reagents and the hydroxyl groups of cellulose. Compared with MA treatment, the crystallinity of cellulose treated by MAMS decreased significantly as increasing the milling time, and the hydrogen bond energy increased significantly as the increase of milling time. It indicates that the addition of metal

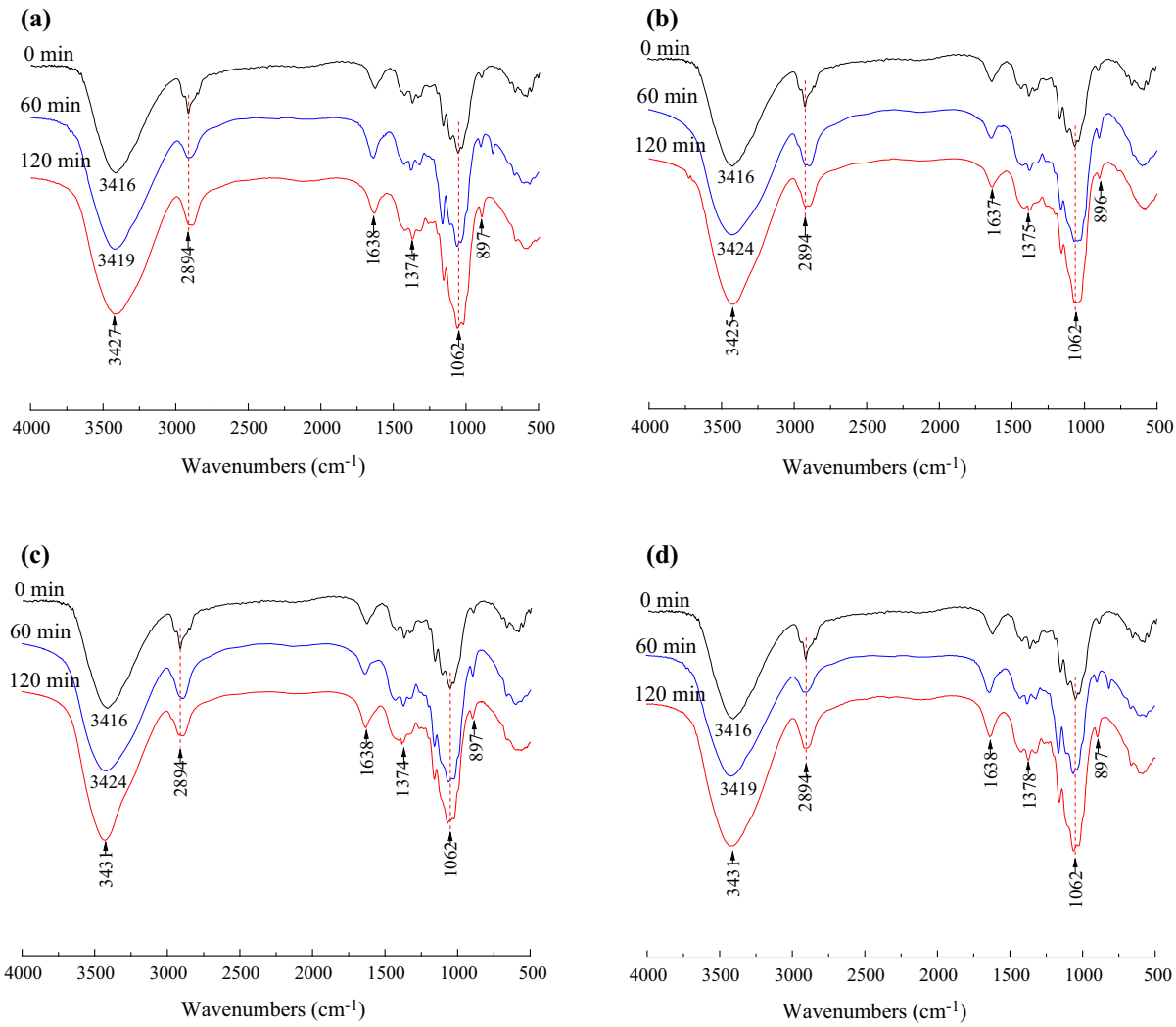

Fig. 3 FTIR spectra of **a** MA treated cellulose, **b** MA + $NaHSO_4$ treated cellulose, **c** MA + $NH_4Fe(SO_4)_2$ treated cellulose, and **d** MA + NaH_2PO_2 treated cellulose

salt could improve the internal energy of cellulose and accelerate the destruction of crystal structure of cellulose by mechanical force. The bands at 2894 and 1062 cm^{-1} assigned to stretching vibration of C–H and –C–O– in cellulose pyranose ring became stronger after MA and MAMS treatments, indicating that the glycosidic bond of cellulose was damaged, and the carbon chain was ruptured by mechanical force. The free hydroxyl groups increased with the increase of milling time, as the peak of O–H stretching vibration shifted to a higher wavenumber and the intensity increased, which is consistent with the result reported by Zhang et al. (2007).

The hydroxyl groups are combined to form intra- and intermolecular hydrogen bonds in the crystalline region of cellulose (Patyk and Katrusiak 2015). According to the literature (Kondo 1997), the characteristic absorption peaks of the intramolecular hydrogen bonds O(2)H…O(6), O(3)H…O(5), and intermolecular hydrogen bond O(6)H…O(3') were at 3455–3410, 3375–3340, and 3310–3230 cm^{-1}, respectively. In order to find out the change in the structure of hydrogen bonds in cellulose by different treatments, Gauss fitting analysis was used for determination, and the results are shown in Table S1. The increase in strength ratio of intramolecular hydrogen bond and the decrease in strength ratio of

Table 2 TCI and ΔE values of untreated and different treated cellulose samples

Sample	TCI (%)	ΔE (ev)
Control	0.56	0
MA treatment[a]	0.44	7.452×10^{-5}
MA treatment[b]	0.29	12.42×10^{-5}
MA + $NaHSO_4$ treatment[a]	0.20	9.936×10^{-5}
MA + $NaHSO_4$ treatment[b]	0.16	14.90×10^{-5}
MA + $NH_4Fe(SO_4)_2$ treatment[a]	0.25	9.936×10^{-5}
MA + $NH_4Fe(SO_4)_2$ treatment[b]	0.18	18.63×10^{-5}
MA + NaH_2PO_2 treatment[a]	0.22	8.69×10^{-5}
MA + NaH_2PO_2 treatment[b]	0.19	18.63×10^{-5}

[a]Milling time = 60 min

[b]Milling time = 120 min

intermolecular hydrogen bond were inconspicuous in the process of MA treatment. It is shown that the hydrogen bonds were destroyed by ball milling, especially the intermolecular hydrogen bonds, and thus increased the content of free hydroxyls. Moreover, some free hydroxyl groups recombined to form intramolecular hydrogen bonds under mechanical force, contributing to the increase in strength ratio of intramolecular hydrogen bond with the increase of milling time. Compared with MA treatment, the strength ratio of intra- and intermolecular hydrogen bonds in the cellulose treated by MAMS rose and fell conspicuously as the increase of milling time, respectively. This suggests that metal salt was diffused into the internal crystalline region of cellulose induced by mechanical force, which helped to enhance the destruction of intermolecular hydrogen bond in cellulose. Therefore, there is a synergistic effect between metal salt and MA.

XRD analysis

XRD measurement is an accurate and effective method to study the crystal structure of cellulose (Nishiyama et al. 2003). The crystal features of MA and MAMS treated cellulose samples were examined by XRD and also compared with the untreated one. The XRD patterns of these cellulose samples are illustrated in Fig. 4. The characteristic diffraction peaks at around $2\theta = 15.10°$, 16.21°, and 22.16° are assigned to (1–10), (110), and (200) planes of cellulose I, respectively (French 2014). The diffraction peaks of control cellulose are sharp with strong intensity, indicating the highly crystal structure of natural cellulose. Figure 4 shows that no new peaks appear in the MA or MAMS treated cellulose, implying that MA or MAMS treatment did not alter the crystalline allomorph of cellulose. The diffraction intensity slowly decreased with increasing the milling time, indicating that the crystalline regions were destroyed by both MA and MAMS treatments. In the XRD patterns of MAMS treated cellulose (Fig. 4b–d), a decrease in the intensity of diffraction peaks and broadening of peaks can be seen obviously compared with those of native cellulose and MA-treated cellulose with the same milling time.

To quantitatively analyze the changes in crystal structure of cellulose after MA and MAMS treatments, crystallinity index (CrI) and D_{200} were calculated based on the corresponding XRD patterns, and the results are shown in Table 3. After MA treatment, CrI and D_{200} of cellulose reduced from 62.88% and 3.81 nm to 21.89% and 1.91 nm after milled for 120 min, respectively. The crystal structure of cellulose was destroyed by the impact of intense ball milling, contributing to the reduction of crystalline unit and the increase of amorphous area in cellulose (Da Silva et al. 2010). However, for this kind of highly crystalline and resistant cellulose, ball milling was difficult to effectively act on its stable crystal structure, so the reduction in CrI of MA treated cellulose was not remarkable. The reduction in CrI and D_{200} of MA + $NaHSO_4$, MA + $NH_4Fe(SO_4)_2$, and MA + NaH_2PO_2 treated cellulose was more remarkable than those of MA treated one. After milled for 120 min, the diffraction patterns of MAMS treated cellulose only exhibit a very broad peak, revealing that MAMS significantly disrupted the inter- and intramolecular hydrogen bonds in cellulose and caused the distortion of crystalline structure. On the one hand, the metal salts were diffused into the crystalline region of cellulose by ball milling, the cations (H^+, Na^+, Fe^{3+}, NH_4^+) and the hydroxyl groups of cellulose combined to form new covalent bonds, which could effectively break the inter- and intramolecular hydrogen bonds (Fischer et al. 2003; Román-Leshkov and Davis 2011). On the other hand, under the instantaneous high temperature induced by collision between milling balls, the metal salts might be in molten state due to their low melting point, which

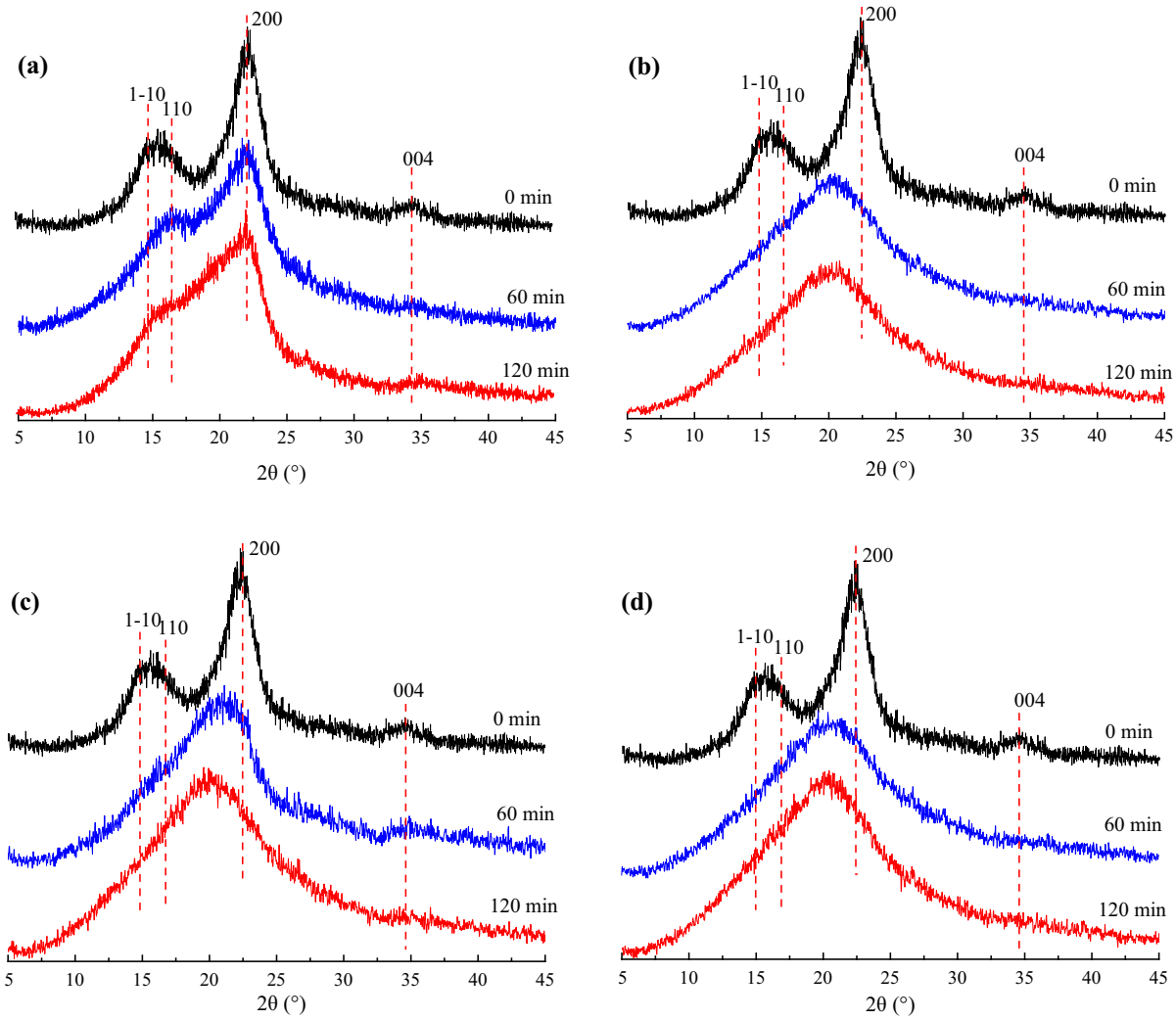

Fig. 4 XRD spectra of **a** MA treated cellulose, **b** MA + $NaHSO_4$ treated cellulose, **c** MA + $NH_4Fe(SO_4)_2$ treated cellulose, and **d** MA + NaH_2PO_2 treated cellulose

was beneficial to accelerate the transfer of energy and the activation of cellulose. Indeed, the crystal structure of cellulose was almost completely destroyed to become amorphous material after 120 min of MAMS treatment. This finding indicates that the addition of three kinds of metal salts enhanced the destruction of crystal structure of cellulose by mechanical force, increasing the accessibility of cellulose, and the best synergistic effect was MA + $NaHSO_4$. As a consequence, during the process of MA and MAMS treatments, intense mechanical actions induced the disruption of strong hydrogen bonding in cellulose and the generation of metastable active sites, which had positive effects on esterification and resulted in the synthesis of maleated cellulose under solid-phase state. It is notable that the catalytic effect of metal salts for esterification of cellulose was not consistent with the synergistic effect of MAMS on crystal structure of cellulose, implying that the change of crystal structure is not a decisive factor for the esterification of cellulose. Thus, it is necessary to further explore the effect of metal salts on the molecular structure of maleic acid.

SEM analysis

The morphological features and surface characteristics of untreated and different treated cellulose

Table 3 CrI and D_{200} values of untreated cellulose and different treated cellulose with different milling time

Sample	CrI (%)	D_{200} (nm)
Control	62.88	3.81
MA treatment[a]	27.55	2.97
MA treatment[b]	21.89	1.91
MA + $NaHSO_4$ treatment[a]	13.62	1.74
MA + $NaHSO_4$ treatment[b]	11.44	1.53
MA + $NH_4Fe(SO_4)_2$ treatment[a]	22.62	1.95
MA + $NH_4Fe(SO_4)_2$ treatment[b]	17.88	1.81
MA + NaH_2PO_2 treatment[a]	21.90	1.97
MA + NaH_2PO_2 treatment[b]	11.78	1.65

[a]Milling time = 60 min

[b]Milling time = 120 min

samples can be clearly observed from SEM micrographs, which are shown in Fig. 5. The surface morphology of highly ordered fibrous structure of original cellulose, composed of compact long fiber microfibrils bundles with smooth surfaces, was significantly changed during MA treatment. After milled for 60 min, the fiber bundles were split and fractured, contributing to the generation of scraps with rough surfaces and notches, but the fiber bundles still can be seen. In comparison, after milled for 120 min, part of the fiber bundles were turned into irregular particles, and a great many of new surfaces were produced, which can be seen in Fig. 5b. The collision, friction, shear, impingement, and other strong mechanical actions between milling balls destroyed the cellulose particles repeatedly, and the fiber bundles were dispersed and broken. Morphologies of the cellulose treated by MA + $NaHSO_4$, MA + $NH_4Fe(SO_4)_2$, and MA + NaH_2PO_2 are shown in Fig. 5c–e. After milled for 60 min, the cellulose microfibrils were split and fractured, contributing to the generation of irregular particles with fluffy and cracky surfaces, and the fibrous structure gradually disappeared. After milled for 120 min, the compact fiber bundle structure was completely destroyed, only leaving small irregular particles, which increased the specific surface area and amorphization of cellulose. The destruction of fibrous structure and increase of specific surface area could provide a facile access of reagents to the hydroxyl groups of cellulose, which increased the chemical reactivity of cellulose and thus enhanced the esterification with maleic acid. The results are in good consistent with those of XRD analysis that metal salts greatly enhanced the destruction on crystal structure of cellulose by mechanical force and thus significantly increase its accessibility.

Effect of metal salts on the structure of maleic acid

FTIR analysis

The MA + $NaHSO_4$ and MA + $NH_4Fe(SO_4)_2$ treated maleic acid were tested by the acid anhydride-hydroxamic acid qualitative test, and the characteristic

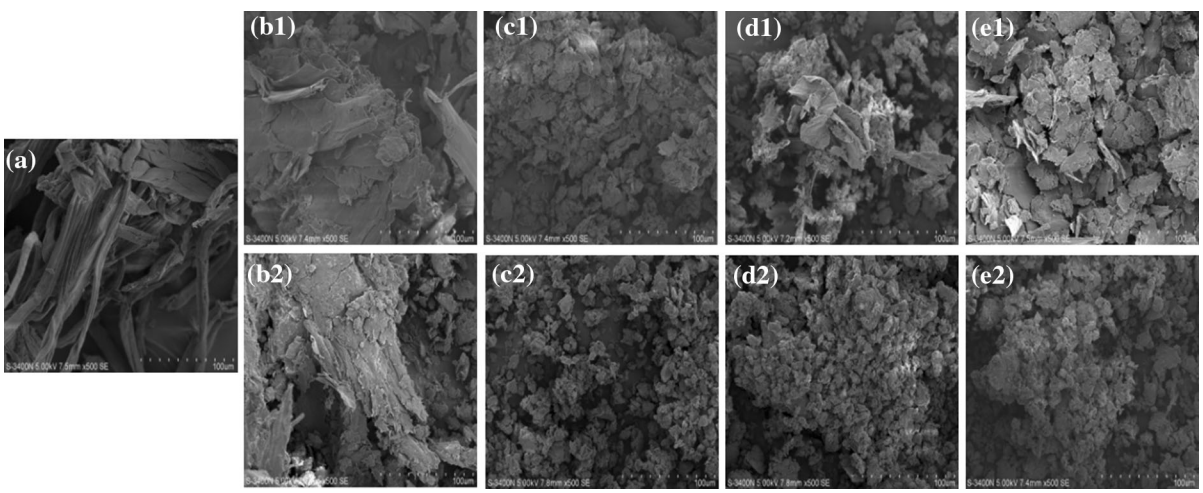

Fig. 5 SEM micrographs of **a** control, **b** MA treated, **c** MA + $NaHSO_4$ treated, **d** MA + $NH_4Fe(SO_4)_2$ treated, and **e** MA + NaH_2PO_2 treated cellulose samples with the milling time of (1) 60 min and (2) 120 min

color (bluish red color) of the hydroxamic acid iron complex compound was not found, indicating that maleic anhydride did not generate during these treatments. Compared with the spectrum of maleic acid in Fig. 6b, the characteristic peaks of acid anhydride at 1850 and 1780 cm^{-1} do not appear in the spectra of Fig. 6c and e, only the characteristic peak of SO_4^{2-} appears at around 1060 cm^{-1}, indicating that maleic acid did not translate to acid anhydride and no new groups were generated or grafted. As showed in Fig. 6c and e, an increase in the intensity of the bands at 3397 and 3422 cm^{-1} corresponding to free O–H band stretching vibration was directly related to the destruction of hydrogen bonds in maleic acid. This demonstrates that the addition of $NaHSO_4$ and $NH_4Fe(SO_4)_2$ enhanced the destruction of hydrogen bonds in maleic acid and improved its reactivity. Therefore, no any new substance was synthesized between maleic acid and these two metal salts in MASPR system, but only the destruction of intermolecular hydrogen bond in maleic acid induced by mechanical force. During the process of MAMS treatment, the chemical reactivity of maleic acid could be enhanced by the addition of $NaHSO_4$ and $NH_4Fe(SO_4)_2$, and thus enhanced the esterification between cellulose and maleic acid.

The MA + NaH_2PO_2 treated maleic acid and fumaric acid were tested by the acid anhydride-hydroxamic acid qualitative test, and then the characteristic color (bluish red color) of the hydroxamic acid iron complex compound was not found, indicating that maleic anhydride did not generate during these treatments. Compared with the spectrum of maleic acid in Fig. 7b, the characteristic peaks of acid anhydride at 1850 and 1780 cm^{-1} do not appear in the spectra of Fig. 7c1–c3, indicating that maleic acid did not translate to acid anhydride. Liquid or solid state carboxylic acids generally formed dipolymers by intermolecular hydrogen bonds. As shown in Fig. 7b, the peak at 3424 cm^{-1} could be assigned to the stretching vibration of intermolecular hydrogen bonds in maleic acid. As shown in Fig. 7c1 and c2, new peaks at 3500 and 3366 cm^{-1} could be ascribed to the bending vibration of intra- and intermolecular hydrogen bonds in maleic acid during the process of MA + NaH_2PO_2 treatment. With the increase of milling time, the peak intensity of the intramolecular hydrogen bonds increased first and then disappeared, while that of the intermolecular hydrogen bonds increased first and then decreased. It obviously confirmed that the intermolecular hydrogen bonds were broken by the synergistic effect between NaH_2PO_2 and mechanical force, and then forming the intramolecular hydrogen bonds. The new stretch at 2427 and 831 cm^{-1} can be caused by P–H stretching vibration of phosphinates. The new band at 1682 cm^{-1} originates from the stretching vibration of C=O in carboxyl and C=C conjugate. The peaks at 1365 and 1219 cm^{-1} result from the in-of-plane bending vibration of O–H and stretching vibration of

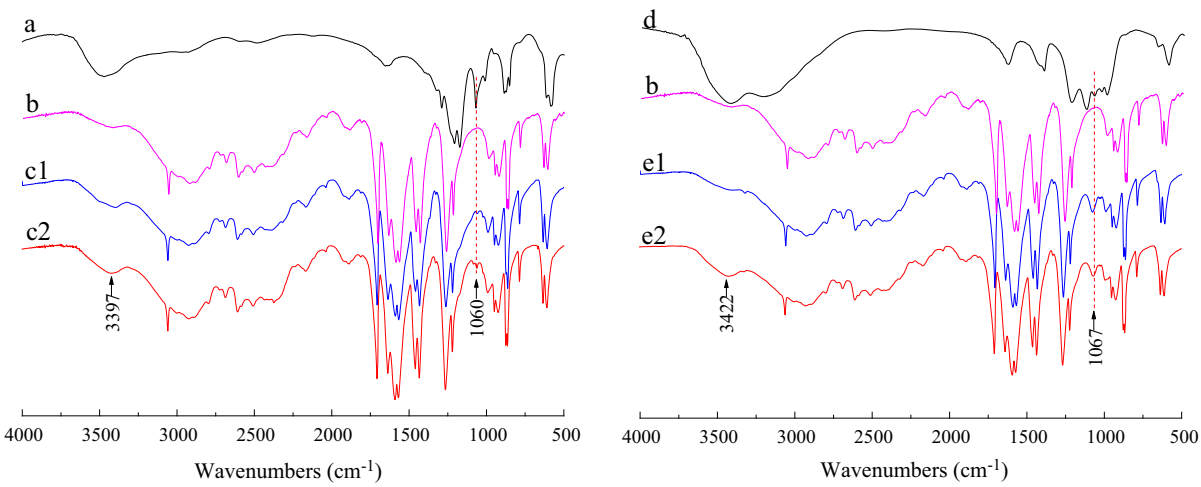

Fig. 6 FTIR spectra of **a** $NaHSO_4$, **b** maleic acid, **c** MA + $NaHSO_4$ treated maleic acid, **d** $NH_4Fe(SO_4)_2$, and **e** MA + $NH_4Fe(SO_4)_2$ treated maleic acid with the milling time of (1) 60 min and (2) 120 min

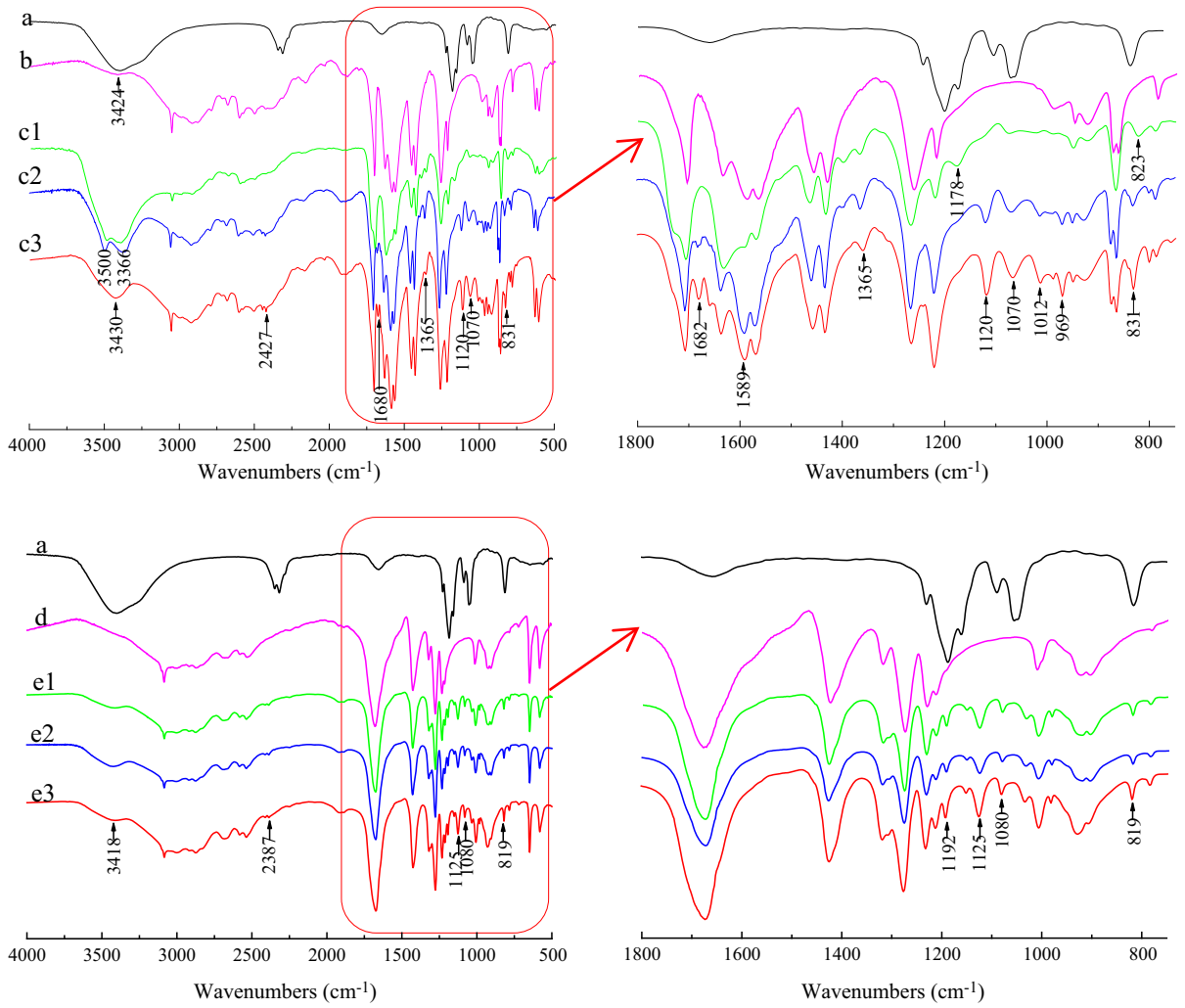

Fig. 7 FTIR spectra of **a** NaH_2PO_2, **b** maleic acid, **c** MA + NaH_2PO_2 treated maleic acid, **d** fumaric acid, **e** MA + NaH_2PO_2 treated fumaric acid with the milling time of (1) 30 min, (2) 60 min, and (3) 120 min

P=O. The bands at 1120, 1070, 1012, and 969 cm^{-1} could be assigned to the symmetrical stretching vibration of P–O–C, while at 831 cm^{-1} could be ascribed to the asymmetric stretching vibration of P–O–C. This demonstrates that an active intermediate was successfully synthesized between maleic acid and NaH_2PO_2 by MASPR.

In order to infer the reaction pathway between maleic acid and cellulose, fumaric acid and NaH_2PO_2 were put in MASPR equipment for testing. Compared with the spectra in Fig. 7a and d, no any new absorption peak appears. As shown in Fig. 7e1–e3, the peaks at 2387, 1125, 1080, and 819 cm^{-1} are attributed to the stretching vibration of the characteristic peaks of NaH_2PO_2, which demonstrates that no new substance was produced between fumaric acid and NaH_2PO_2 by MASPR. The results confirm that fumaric acid could not form intramolecular hydrogen bonds because of the steric effect of hydroxyl groups located on the opposite side of C=C bond. However, maleic acid could form intramolecular hydrogen bonds because the hydroxyl groups of maleic acid is located on the same side of C=C bond, with the highest degree of cis-stereoselectivity. Therefore, the intermolecular hydrogen bonds of maleic acid could be destroyed by the addition of NaH_2PO_2 in MASPR system, promoting the formation of intramolecular hydrogen bonds.

^{31}P-NMR analysis

The structure of phosphorus compounds was examined by ^{31}P-NMR measurement, which is an effective and ideal technique (Charmot and Katz 2010; Condron et al. 1985). In order to further confirm the structure of active intermediates formed between maleic acid and NaH_2PO_2 by MASPR, the chemical structure of the phosphorus compounds milled for 120 min was investigated by ^{31}P-NMR, and the result is presented in Fig. 8. As shown in Fig. 8a and c, the signals at 7.246 and 2.718 ppm correspond to the signals of P=O and P–H, respectively, demonstrating that chemical reaction between fumaric acid and NaH_2PO_2 did not take place by MASPR, and thus no active intermediate generated. As shown in Fig. 8b, a new peak at 5.813 ppm originates from the signal of P–O–C, indicating that an active intermediate could be successfully synthesized between maleic acid and NaH_2PO_2 by ball milling.

Catalytic mechanism of metal salts for esterification of cellulose by MASPR

Based on the analyses of XRD, FTIR, SEM, and ^{31}P-NMR, the catalytic mechanism of these three metal salts for esterification of cellulose in MASPR system can be divided into two aspects. One is that the synergistic effect of MA and metal salt on cellulose, and the other is the effect of MA and MAMS on the molecular structure of maleic acid.

Effect of MA and MAMS on cellulose

Based on the comprehensive analyses of XRD, FTIR, and SEM, it can be found that the presence of metal salts helped to enhance the destruction in crystalline structure of cellulose by ball milling. This may due to that the oxygen atoms of the hydroxyl groups connected with C-2, C-3 and C-6 in pyranose ring monomers of cellulose are more active and polar, and O-5 also shows polarity, which led to easy adsorption of metal ions. According to the combination relationship of some metal ions and cellulose (Nowakowski et al. 2008; Saddawi et al. 2012), we hypothesize the combination relationship between cellulose and metal ions in MASPR system, which is shown in Scheme 1. The glycosidic bonds between pyranose rings in cellulose were first destroyed by ball milling, contributing to the damage of carbon chain and crystalline region and the increase of amorphous region. Then, the cations, H^+, Na^+, NH_4^+, and Fe^{3+}, combined with the hydroxyl oxygen atoms on the surface of cellulose, and the electrons of carbon atoms and oxygen atoms of

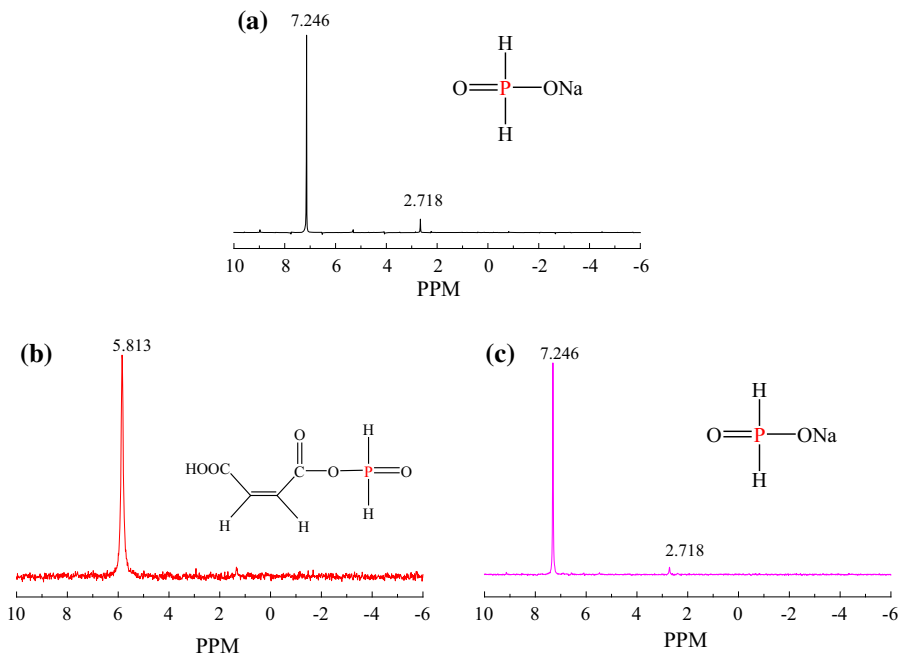

Fig. 8 ^{31}P-NMR spectra of **a** NaH_2PO_2, **b** MA + NaH_2PO_2 treated maleic acid (milling time = 120 min), and **c** MA + NaH_2PO_2 treated fumaric acid (milling time = 120 min)

Scheme 1 Mechanism scheme of the effect of metal salts on cellulose

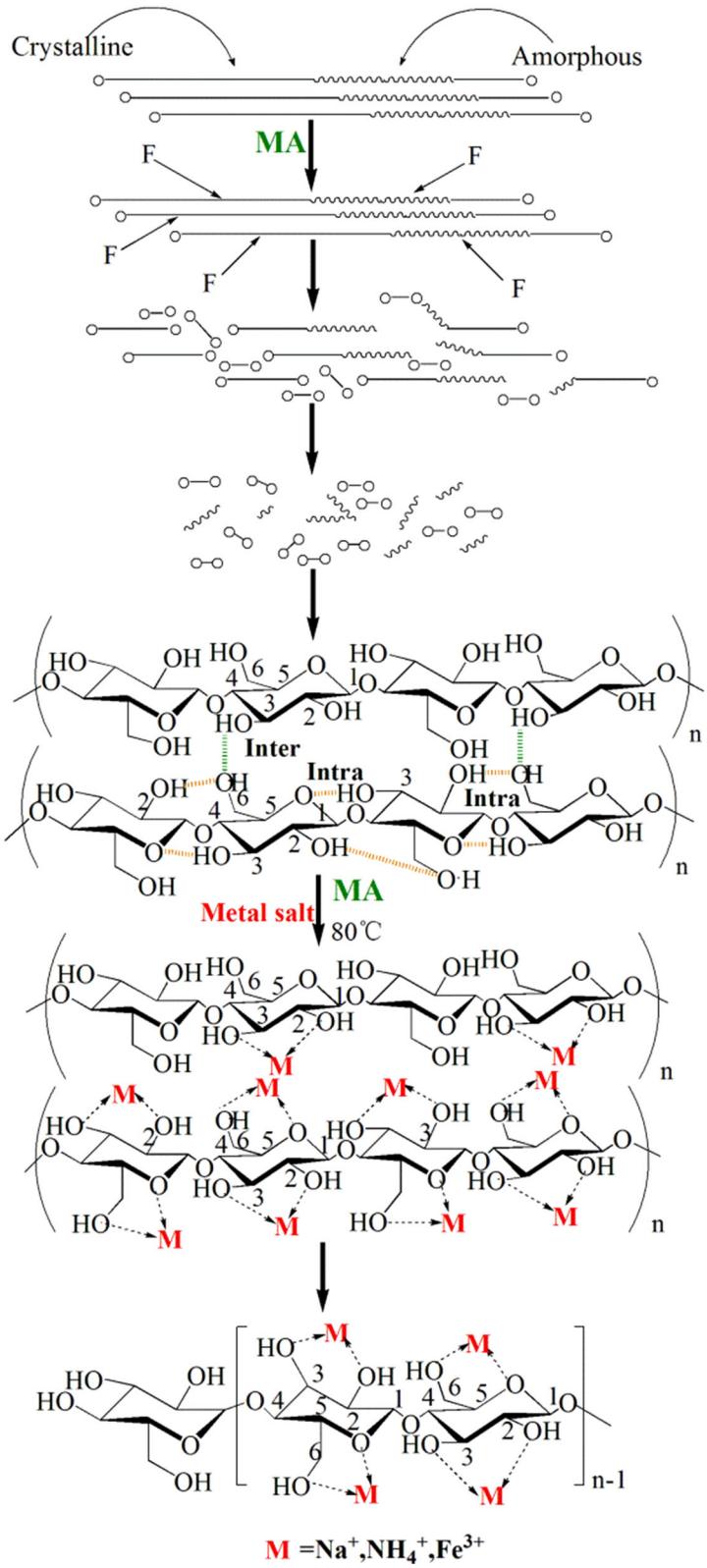

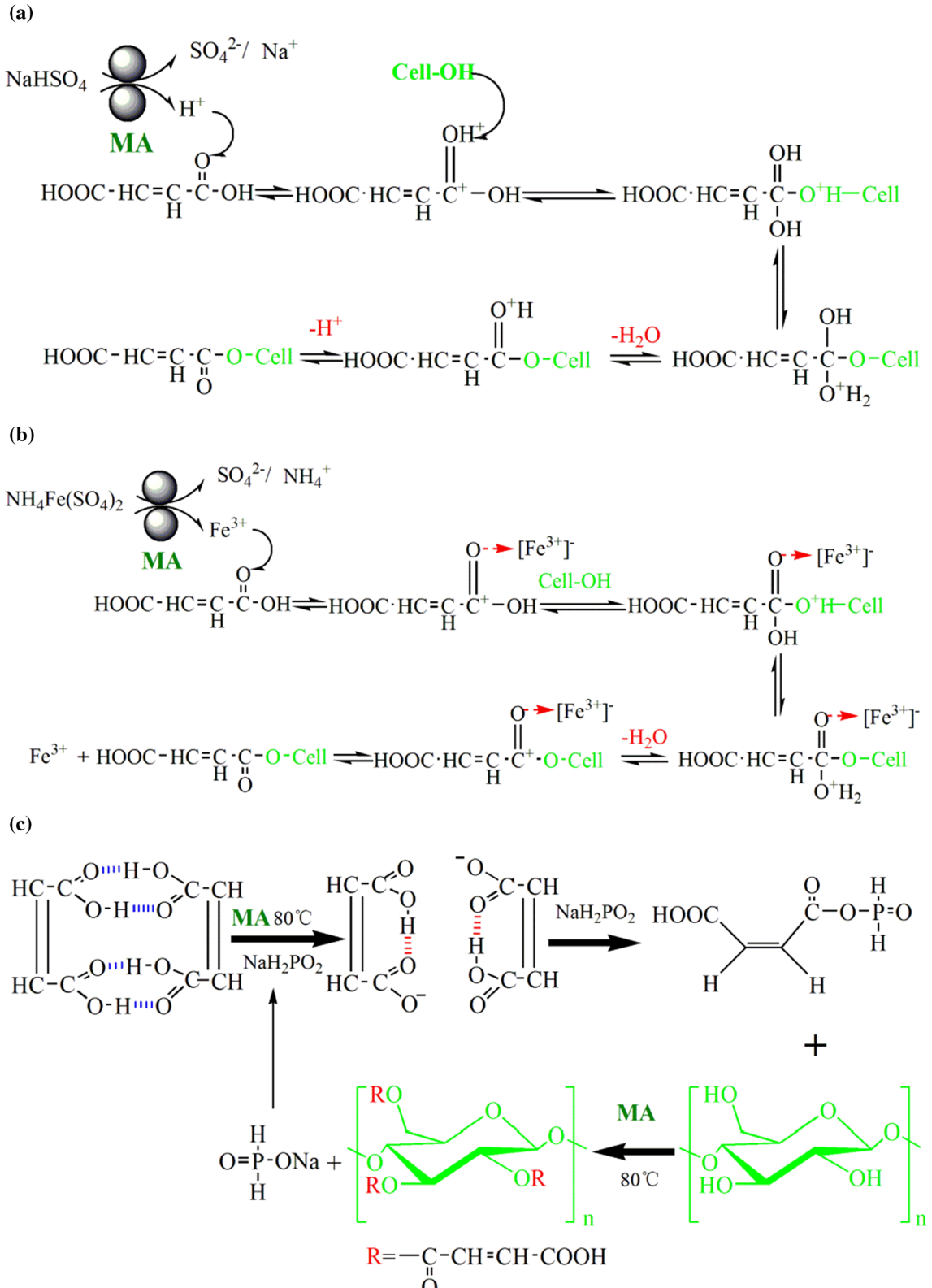

Scheme 2 The catalytic mechanism schemes of **a** $NaHSO_4$, **b** $NH_4Fe(SO_4)_2$, and **c** NaH_2PO_2

the pyranose ring were impacted in different extent by the adsorption of cations, resulting in the change in bond angle of C–C and C–O, increase of bond length, deformation of pyranose ring, and weakening of inter- and intermolecular hydrogen bonds in cellulose. Moreover, the compact structure of cellulose was destroyed by the mechanical force, contributing to that the inter- and intramolecular hydrogen bonds were weakened and even destroyed, which is confirmed in infrared spectra that the peak of O–H stretching vibration shifted to a higher wavenumber and the peak intensity increased. As the crystalline region of cellulose was destroyed and the amorphous area increased, cellulose was in a highly amorphous state. The destruction of stable structure of cellulose increases its accessibility, which can enhance the esterification of cellulose with maleic acid.

Effect of MA and MAMS on maleic acid

The catalytic mechanism scheme of $NaHSO_4$ is illustrated in Scheme 2a. $NaHSO_4$ contains a water of crystallization, which would promote the surface ionization of $NaHSO_4$ to ionize H^+ ions under the collision and squeezing between milling balls, leading to the higher electropositive of carboxyl carbon atoms. It is beneficial for the hydroxyl groups of cellulose to attack these H^+ ions. The central carbon atom occurred sp^3 hybridized to form a tetrahedral intermediate, and then the proton was transferred, following by the loss of one molecule of water and hydrogen ion to generate maleated cellulose. With the progress of catalytic reaction, the generated water made $NaHSO_4$ to ionize more H^+, which could accelerate the esterification. Clearly, the catalytic mechanism of $NaHSO_4$ belonged to that of protonic acid.

The catalytic mechanism of $NH_4Fe(SO_4)_2$ is expounded in Scheme 2b. The melting point of $NH_4Fe(SO_4)_2$ is 39–41 °C, so it was in molten state under the milling temperature of 80 °C, and the lattice would be destroyed and have a higher activity. In addition, the Fe^{3+}, NH_4^+, and SO_4^{2-} ions in $NH_4Fe(SO_4)_2$ were ionized by the collision and extrusion of milling balls. Fe^{3+} has empty "d" orbitals, which can coordinate with the lone pair of electron in the carbonyl oxygen. Therefore, the electron cloud of C=O in the carbonyl groups strongly biases toward the oxygen atoms, reducing its activation energy and generating a proton acid center, which has catalytic action. In the process of MASPR, Fe^{3+} was ionized from $NH_4Fe(SO_4)_2$ induced by ball milling, and the Fe^{3+} ion coordinated with the lone pair of electron in carbonyl oxygen to form an intermediate, following by proton transfer and the loss of one molecule of water, and then maleated cellulose was successfully produced. Therefore, the catalytic mechanism of $NH_4Fe(SO_4)_2$ belonged to that of Lewis acid.

In liquid phase, the catalytic mechanism of NaH_2PO_2 is considered to be carried out in two steps reaction process: first, cyclic anhydrides are formed as intermediates by dehydrating between hydroxyls in polycarboxylic acids; second, esters are produced by substitution reaction between hydroxyls of cellulose and cyclic anhydrides (Morris et al. 1996). Herein, the catalytic mechanism of NaH_2PO_2 is clarified in Scheme 2c. Firstly, the intermolecular hydrogen bonds between the molecules of maleic acid could be weakened by the addition of NaH_2PO_2 under ball milling, which promoted the formation of intramolecular hydrogen bonds and was further conducive to the reaction. Then, an active intermediate was formed between maleic acid and NaH_2PO_2 induced by ball milling, and the hydroxyl groups of cellulose were attacked by the active intermediate. Finally, maleated cellulose and NaH_2PO_2 were successfully formed by the nucleophilic substitution reaction between active intermediate and the hydroxyl groups of cellulose, and NaH_2PO_2 continued to act as a catalyst for esterification.

Conclusions

Three metal salts, sodium bisulfate, ammonium ferric sulfate, and sodium hypophosphite, possessed good catalytic effects for the esterification of cellulose in MASPR system. XRD, FTIR, and SEM analyses confirmed that the assistance of metal salts in MA treatment had positive effect on the structure changes of cellulose. Comparative studies of MA and MAMS treatments indicated that the combination of MA and metal salts exhibited synergistic effect for more effective changes of the structural characteristics of cellulose. In addition, the changes in chemical structure of maleic acid before and after MAMS treatment showed that no active intermediate formed between maleic acid and $NaHSO_4$ or $NH_4Fe(SO_4)_2$ by MASPR. Therefore, the catalytic mechanism of $NaHSO_4$ and

$NH_4Fe(SO_4)_2$ belonged to that of protonic acid and Lewis acid, respectively. The catalytic mechanism of NaH_2PO_2 was considered as that it could react with maleic acid to form active intermediates under ball milling, and then the active intermediates reacted with hydroxyl groups of cellulose. Hopefully, the detailed investigation on catalytic mechanism of metal salts for the esterification of cellulose in MASPR system is of great significance for the solid phase modification of polysaccharide polymers.

Acknowledgments This research was supported by National Natural Science Foundation of China (Nos. 51463003 and 21666005), the Guangxi Science and Technology Plan Project of China (Grant No. AB16380305), Guangxi Distinguished Experts Special Foundation of China, and the Scientific Research Foundation of Guangxi University (Grant No. XJPZ160713).

References

Abhilash PC, Singh N (2008) Influence of the application of sugarcane bagasse on lindane (γ-HCH) mobility through soil column: implication for biotreatment. Bioresour Technol 99(18):8961–8966

Barbosa SL, Dabdoub MJ, Hurtado GR, Klein SI, Baroni ACM, Cunha C (2006) Solvent free esterification reactions using Lewis acids in solid phase catalysis. Appl Catal A-Gen 313(2):146–150

Bassan IAL, Nascimento DR, San Gil RAS, Pais Da Silva MI, Moreira CR, Gonzalez WA Jr, Faro AC, Onfroy T, Lachter ER (2013) Esterification of fatty acids with alcohols over niobium phosphate. Fuel Process Technol 106:619–624

Cao X, Sun S, Peng X, Zhong L, Sun R, Jiang D (2013) Rapid synthesis of cellulose esters by transesterification of cellulose with vinyl esters under the catalysis of NaOH or KOH in DMSO. J Agric Food Chem 61(10):2489–2495

Charmot A, Katz A (2010) Unexpected phosphate salt-catalyzed hydrolysis of glycosidic bonds in model disaccharides: cellobiose and maltose. J Catal 276(1):1–5

Chundawat SPS, Bellesia G, Uppugundla N, Da Costa Sousa L, Gao D, Cheh AM, Agarwal UP, Bianchetti CM, Phillips GN, Langan P, Balan V, Gnanakaran S, Dale BE (2011) Restructuring the crystalline cellulose hydrogen bond network enhances its depolymerization rate. J Am Chem Soc 133(29):11163–11174

Condron LM, Goh KM, Newman RH (1985) Nature and distribution of soil phosphorus as revealed by a sequential extraction method followed by ^{31}P nuclear magnetic resonance analysis. Eur J Soil Sci 36(2):199–207

Cr Py L, Chaveriat L, Banoub J, Martin P, Joly N (2009) Synthesis of cellulose fatty esters as plastics-influence of the degree of substitution and the fatty chain length on mechanical properties. ChemSusChem 2(2):165–170

Crawford D, Casaban J, Haydon R, Giri N, McNally T, James SL (2015) Synthesis by extrusion: continuous, large-scale preparation of MOFs using little or no solvent. Chem Sci 6(3):1645–1649

Da Silva ASA, Inoue H, Endo T, Yano S, Bon EPS (2010) Milling pretreatment of sugarcane bagasse and straw for enzymatic hydrolysis and ethanol fermentation. Bioresour Technol 101(19):7402–7409

Dankovich TA, Hsieh Y (2007) Surface modification of cellulose with plant triglycerides for hydrophobicity. Cellulose 14(5):469–480

Fischer S, Leipner H, Thummler K, Brendler E, Peters J (2003) Inorganic molten salts as solvents for cellulose. Cellulose 10(3):227–236

French AD (2014) Idealized powder diffraction patterns for cellulose polymorphs. Cellulose 21(2):885–896

Fumagalli M, Ouhab D, Boisseau SM, Heux L (2013) Versatile gas-phase reactions for surface to bulk esterification of cellulose microfibrils aerogels. Biomacromol 14(9):3246–3255

Gillingham EL, Lewis DM, Voncina B (1999) An FTIR study of anhydride formation on heating butane-tetracarboxylic acid in the presence of various catalysts. Text Res J 69(12):949–955

Granstrom M, Kavakka J, King A, Majoinen J, Makela V, Helaja J, Hietala S, Virtanen T, Maunu S, Argyropoulos DS, Kilpelainen I (2008) Tosylation and acylation of cellulose in 1-allyl-3-methylimidazolium chloride. Cellulose 15(3):481–488

Granstrom M, Paakko MKN, Jin H, Kolehmainen E, Kilpelainen I, Ikkala O (2011) Highly water repellent aerogels based on cellulose stearoyl esters. Polym Chem 2(8):1789–1796

Hu H, Li H, Zhang Y, Chen Y, Huang Z, Huang A, Zhu Y, Qin X, Lin B (2015) Green mechanical activation-assisted solid phase synthesis of cellulose esters using a co-reactant: effect of chain length of fatty acids on reaction efficiency and structure properties of products. RSC Adv 5(27):20656–20662

Huang K, Wang B, Cao Y, Li H, Wang J, Lin W, Mu C, Liao D (2011) Homogeneous preparation of cellulose acetate propionate (CAP) and cellulose acetate butyrate (CAB) from sugarcane bagasse cellulose in ionic liquid. J Agric Food Chem 59(10):5376–5381

Huang Z, Tan Y, Zhang Y, Liu X, Hu H, Qin Y, Huang H (2012a) Direct production of cellulose laurate by mechanical activation-strengthened solid phase synthesis. Bioresour Technol 118:624–627

Huang Z, Wang N, Zhang Y, Hu H, Luo Y (2012b) Effect of mechanical activation pretreatment on the properties of sugarcane bagasse/poly(vinyl chloride) composites. Compos part A-Appl S 43(1):114–120

James SL, Adams CJ, Bolm C, Braga D, Collier P, Friscic T, Grepioni F, Harris KD, Hyett G, Jones W, Krebs A, Mack J, Maini L, Orpen AG, Parkin IP, Shearouse WC, Steed JW, Waddell DC (2012) Mechanochemistry: opportunities for new and cleaner synthesis. Chem Soc Rev 41(1):413–447

Jr. Karnitz O, Alves Gurgel LV, Perin De Melo JC, Botaro VR, Sacramento Melo TM, de Freitas Gil RP, Gil LF (2007) Adsorption of heavy metal ion from aqueous single metal solution by chemically modified sugarcane bagasse. Bioresour Technol 98(6):1291–1297

Kim D, Moreno N, Nunes SP (2016) Fabrication of polyacrylonitrile hollow fiber membranes from ionic liquid solutions. Polym Chem 7(1):113–124

Kondo T (1997) The assignment of IR absorption bands due to free hydroxyl groups in cellulose. Cellulose 4(4):281–292

Lam E, Luong JHT (2014) Carbon materials as catalyst supports and catalysts in the transformation of biomass to fuels and chemicals. ACS Catal 4(10):3393–3410

Leng Y, Wang J, Zhu D, Ren X, Ge H, Shen L (2009) Heteropolyanion-based ionic liquids: reaction-induced self-separation catalysts for esterification. Angew Chem Int Edit 48(1):168–171

Morales-delaRosa S, Campos-Martin JM, Fierro JLG (2014) Complete chemical hydrolysis of cellulose into fermentable sugars through ionic liquids and antisolvent pretreatments. ChemSusChem 7(12):3467–3475

Morán JI, Alvarez VA, Cyras VP, Vázquez A (2008) Extraction of cellulose and preparation of nanocellulose from sisal fibers. Cellulose 15(1):149–159

Morris CE, Morris NM, TraskMorrell BJ (1996) Interaction of meso-1,2,3,4-butanetetracarboxylic acid with phosphorus-containing catalysts for esterification cross-linking of cellulose. Ind Eng Chem Res 35(3):950–953

Nishiyama Y, Langan P, Chanzy H (2002) Crystal structure and hydrogen-bonding system in cellulose I_β from synchrotron X-ray and neutron fiber diffraction. J Am Chem Soc 124(31):9074–9082

Nishiyama Y, Sugiyama J, Chanzy H, Langan P (2003) Crystal structure and hydrogen bonding system in cellulose I_α from synchrotron X-ray and neutron fiber diffraction. J Am Chem Soc 125(47):14300–14306

Nowakowski DJ, Woodbridge CR, Jones JM (2008) Phosphorus catalysis in the pyrolysis behaviour of biomass. J Anal Appl Pyrol 83(2):197–204

Patyk E, Katrusiak A (2015) Transformable H-bonds and conformation in compressed glucose. Chem Sci 6(3):1991–1995

Román-Leshkov Y, Davis ME (2011) Activation of carbonyl-containing molecules with solid Lewis acids in aqueous media. ACS Catal 1(11):1566–1580

Rowell RM (1994) Acetyl distribution in acetylated whole wood and reactivity of isolated wood cell-wall components to acetic anhydried. Wood Fiber Sci 26(1):11–18

Saddawi A, Jones JM, Williams A (2012) Influence of alkali metals on the kinetics of the thermal decomposition of biomass. Fuel Process Technol 104:189–197

Sehaqui H, Kulasinski K, Pfenninger N, Zimmermann T, Tingaut P (2017) Highly carboxylated cellulose nanofibers via succinic anhydride esterification of wheat fibers and facile mechanical disintegration. Biomacromol 18(1):242–248

Sun RC, Tomkinson J, Wang SQ, Zhu W (2000) Characterization of lignins from wheat straw by alkaline peroxide treatment. Polym Degra. Stabil 67(1):101–109

Uschanov P, Johansson L, Maunu SL, Laine J (2011) Heterogeneous modification of various celluloses with fatty acids. Cellulose 18(2):393–404

Zhang W, Liang M, Lu C (2007) Morphological and structural development of hardwood cellulose during mechanochemical pretreatment in solid state through pan-milling. Cellulose 14(5):447–456

Zhang Y, Gan T, Luo Y, Zhao X, Hu H, Huang Z, Huang A, Qin X (2014) A green and efficient method for preparing acetylated cassava stillage residue and the production of all-plant fibre composites. Compos Sci Technol 102:139–144